IOPscience iopscience.iop.org

Home Search Collections Journals About Contact us My IOPscience

Studies of structural arrest transition in L64/D_2O micellar solutions

This article has been downloaded from IOPscience. Please scroll down to see the full text article.

2004 J. Phys.: Condens. Matter 16 S4951

(http://iopscience.iop.org/0953-8984/16/42/012)

View the table of contents for this issue, or go to the journal homepage for more

Download details:
IP Address: 129.252.86.83
The article was downloaded on 27/05/2010 at 18:21

Please note that terms and conditions apply.

INSTITUTE OF PHYSICS PUBLISHING JOURNAL OF PHYSICS: CONDENSED MATTER

J. Phys.: Condens. Matter **16** (2004) S4951–S4974 PII: S0953-8984(04)79466-7

Studies of structural arrest transition in L64/D_2O micellar solutions

Wei-Ren Chen[1], **Yun Liu**[1], **Francesco Mallamace**[1,2], **Pappannan Thiyagarajan**[3] **and Sow-Hsin Chen**[1,2]

[1] Department of Nuclear Engineering, Massachusetts Institute of Technology, Cambridge, MA 02139-4307, USA
[2] Dipartimento di Fisica e Istituto Nazionale per la Fisica della Materia, Universita' di Messina, Messina, Italy
[3] IPNS Division, Argonne National Laboratory, Argonne, IL 60439, USA

Received 14 April 2004
Published 8 October 2004
Online at stacks.iop.org/JPhysCM/16/S4951
doi:10.1088/0953-8984/16/42/012

Abstract

We summarize the results of analyses of a series of small angle neutron scattering (SANS) experiments on dense L64 copolymer micellar solutions in heavy water. The system is modelled as a suspension of micellar particles that interact among themselves with a hard core plus a short range square well attractive interaction. The observed phase behaviour in the plane of temperature and polymer concentration is described. Characteristic features such as the existence of the glass-to-liquid-to-glass re-entrance transition and the line of glass-to-glass transition with its associated end point (A_3 singularity) are found which are quantitatively consistent with the recent mode coupling theory calculations using the same model potential. Supplementary to SANS experiments, photon correlation spectroscopy experiments on the same system have been performed. They show that although the Debye–Waller factors (the long time limits of the coherent intermediate scattering functions) of the two glasses do indeed become identical at the A_3 point as predicted, the intermediate scattering functions exhibit distinctly different intermediate time relaxations. Furthermore, we show that the Debye–Waller factors obtained from volume fractions beyond the A_3 point have the same magnitude as for the repulsive glass obtained before the A_3 point. In addition, the effect of applied pressure on the kinetic glass transition (KGT) is explored for the first time. We observe that, for the KGT in L64/D_2O micellar system, increasing applied pressure at constant temperature has a similar effect to reducing temperature at constant pressure. The preliminary observation of the ageing effect on quenching into the attractive glass state with the SANS technique is reported as well.

(Some figures in this article are in colour only in the electronic version)

 © 2004 IOP Publishing Ltd Printed in the UK

1. Introduction

In the material world in which we are living, there are abundant colloidal systems. Our daily life is surrounded by materials made of colloids, that either occurred naturally or were prepared artificially [1]: examples include inorganic materials such as inks and paints; many foodstuffs, such as milk and yogurt, which can provide the proteins required for everyday life; even the very stuff we are made of, such as cells, blood and bones, also contains colloidal particles.

Despite the diversity of the colloidal systems, in general they share a unique feature: unlike the case for atomic or molecular systems, the potential of interaction among the colloidal particles is in general short ranged—that is, small compared to the particle size. Colloids exhibit a rich variety of phase behaviours: for example, the existence of liquid–liquid phase separation, e.g. a binodal line with the associated critical point, and the percolation transition line. These phenomena can be traced back to some of the manifestations of the short range nature of the interaction potential. Figure 1 gives an example of a phase diagram of such a complex liquid: the L64/D_2O micellar solution which is the main focus of this paper.

Among all the different regions of the phase diagram, probably that where structural arrest states (glassy states) exist is the most interesting one. They are observed in many colloidal systems and their vital importance to our daily life is reflected in the following list: glue, shampoo, and medical oral gel are all examples of glassy states. However, despite their ubiquity, their scientific investigation is a recent development. Although the structural arrest states are amorphous states of soft matter, they are notoriously ill-characterized structurally and dynamically: they cannot be categorized as gaseous, liquid or crystalline states.

During the last decade, a number of theoretical explanations based on a thermodynamic perspective have been proposed to interpret their physical nature. Examples include the percolation transition and the liquid-to-solid transition. However, when compared with experimental evidence, none of them is completely satisfactory. On the other hand, from a kinetic viewpoint, if a liquid has been supercooled below the melting point without this resulting in crystallization, the dynamics of its constituting particles will slow down dramatically and eventually its structure will be frozen. Instead of a transition into a crystalline solid, the true equilibrium ground state, it undergoes a so-called structural arrest transition or kinetic glass transition (KGT) and turns into an amorphous glassy state, in which the local particle configuration deviates from the thermodynamical equilibrium state and its motion is hindered by the presence of a long lived cage formed by its neighbours. If one admits its nonergodic nature, the transition which causes the colloidal system to transform into an amorphous state can be regarded as a consequence of a KGT. By studying the liquid–glass transition in a colloidal system interacting via a short ranged attractive interaction, recent mode coupling theory (MCT) calculations [2] provide a promising theoretical tool for drawing a fundamental coherent picture of this familiar yet ill-defined phenomenon.

The KGT in supercooled liquids has been studied extensively in the past two decades [3–5]. For a class of systems in which the potential of interaction among the particles can be modelled as a hard sphere interaction, many valuable insights into the physics of the KGT have resulted from the ideal MCT calculations. The major theoretical predictions are summarized as follows: at low volume fractions, the behaviour of the hard sphere system is fluid-like. As the volume fraction increases, the test particle time correlation function (self-ISF) and the density–density correlation function (ISF) of the particles exhibit a two-stage relaxation process. The initial decay of the self-ISF corresponds to rattling of a typical particle confined within a transient cage formed by its neighbours, followed by a slow decay, resulting from relaxation of the cage itself and the escape of the trapped particle by rearranging its nearest neighbour configuration. The latter process leads to the possibility of particle diffusion through coupling to the structural

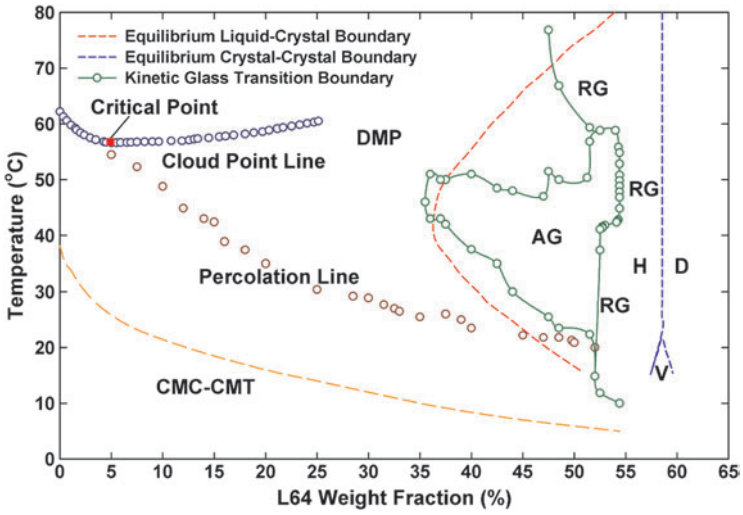

Figure 1. The phase diagram (in the temperature–weight fraction plane) of Pluronic L64 in D_2O solution. The phase diagram contains the CMC–CMT line, cloud point line, critical point, percolation line, equilibrium liquid-to-hexagonal liquid crystal phase boundary (long dashed line), equilibrium crystal-to-crystal phase boundary (short dashed line) and re-entrant KGT lines, separating the liquid phase and two different glasses. H, D and V represent hexagonal, lamellar and cubic phases respectively.

relaxation process. The system will be dynamically much slower when its volume fraction is near a certain value, beyond which the system will be 'arrested' in an amorphous state, rather than condensing into a crystal.

The experimental results show that the application of the KGT to colloidal systems is highly successful. If a spherical colloidal system is treated as a hard sphere fluid physically, the connection can be seen explicitly. For a spherical colloidal system, at volume fractions of less than 0.49, only the fluid is found. Between 0.49 and 0.55 the equilibrium state is two-phase coexistence of a fluid and an FCC crystal. However, if one is able to manipulate a colloidal system to avoid crystallization at the volume fraction of 0.49, for example by artificially creating a polydispersity in sizes of a few per cent, at a critical volume fraction ϕ_c, which was predicted to be 0.516 (but determined to be 0.58 experimentally), the KGT can be observed [6]. At the KGT, both the particle diffusion and the long time density fluctuations freeze and the system undergoes an ergodic-to-nonergodic transition. Although this characteristic feature has been confirmed by computer molecular dynamics simulations [7] and laboratory experiments [6, 8] involving several model hard sphere systems, there have been some anomalous dynamical observations, which cannot be interpreted in terms of the theory based on the hard sphere potential alone [9].

It is natural to ask whether a more complete picture of the KGT can be obtained by modelling the interparticle potential more accurately. The answer stems from a slight modification of the hard sphere interaction potential and has been attracting a great deal of attention lately. Recent MCT calculations [10–12] show that if a system is characterized by a hard core plus an additional short range attractive interaction—for example, by an adhesive hard sphere system (AHS)—a different structural arrest scenario emerges. Theoretically, the phase behaviour of the AHS is characterized by an effective temperature $T^* = k_B T/u$, the volume fraction of the particles ϕ and the fractional attractive well width $\varepsilon = \Delta/R$, where $-u$ is the depth of the attractive square well, Δ the width of the well and R the diameter of

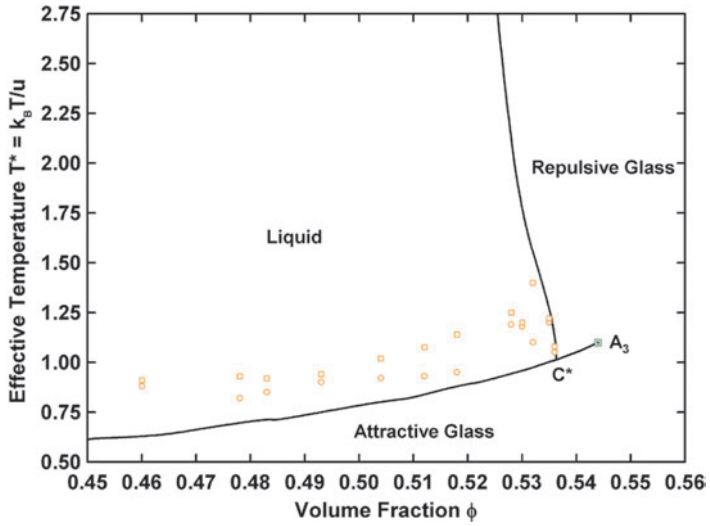

Figure 2. The theoretical phase diagram predicted by MCT calculations using the short range attractive square well potential with $\varepsilon = 0.03$. The calculations predict the attractive glass-to-liquid-to-repulsive glass re-entrant transition, the attractive glass-to-repulsive glass transition and the end point of the glass–glass transition line. Symbols (circles and squares) represent the effective temperature T^*, determined by fitting the experimental SANS data taken in the liquid state with the method explained in the text.

the particle. In this case, for a given ε, in addition to the volume fraction, a second external control parameter, the effective temperature T^*, is introduced into the description of the phase behaviour of the system and the loss of ergodicity can take place either by increasing the volume fraction or by changing the effective temperature.

Figure 2 gives part of the predicted phase diagram based on the AHS with $\varepsilon = 0.03$. In this case, it is possible for the system to undergo a re-entrant (glass-to-liquid-to-glass) transition on varying the effective temperature. At high effective temperatures and at sufficiently high volume fractions, the system evolves into the well-known structurally arrested (glassy) state, called a 'repulsive glass', as a result of the cage effect, a manifestation of the excluded volume effect due to the existence of the hard core. However, at relatively low effective temperatures, an 'attractive glass' can form in which the motion of the typical particle is constrained instead by cluster formation with neighbouring particles. Moreover, in an AHS, in addition to the hard core diameter, the range of the attractive well should come into play (parameter ε). The MCT calculations show that, with sufficiently small ε, variation of the two control parameters, T^* and ϕ, allows a transition between these two distinct forms of glass. Thus there is a branch of the KGT line across which transitions between the attractive glass and the repulsive glass are predicted. Of particular interest is the occurrence of an A_3 singularity at which point the glass-to-glass transition line terminates. MCT suggests that the long time dynamics of the two distinct structurally arrested states become identical at and beyond this point.

Several ongoing experimental investigations have confirmed some of the theoretical predictions, such as the re-entrant glass-to-liquid-to-glass transition phenomenon [13, 14] and the logarithmic relaxation of the glassy dynamics in the liquid states in the vicinity of the A_3 singularity [15], which are considered to be the signatures of the glassy dynamics in the two-length-scale system. More recently, a series of experimental investigations focusing on a dense micellar system gave the first report of the glass-to-glass transition line and its associated end point and the detailed analysis leads to physical insight into the slow dynamics in the two

glassy states [16, 17, 19]. The satisfactory agreement between experimental results and MCT calculations for an AHS justifies treating the L64/D_2O micellar systems within the framework of the glass transition.

As mentioned in our reports [16, 17, 19], above the CMC–CMT line, the decreasing solubility of D_2O solvent molecules in PEO corona as temperature increases leads to attraction between the micelles. When two micelles touch each other, some D_2O molecules in the corona region are squeezed out and the overlapping between the PEO coronas of two micelles gives rise to the characteristic of short range intermicelle attraction [21]. More specifically, there are two different hydrogen bonds existing in the system: the hydrogen bonds among D_2O molecules and the hydrogen bonds between D_2O molecules and L64 polymers. It is clear that the responses of these two hydrogen bonds to the thermal fluctuation are different and the increasing short range attraction can be viewed as the consequence of the interplay between these two hydrogen bond networks as a function of temperature. All the observed phase behaviours discovered in our research, such as the liquid-to-glass transition and glass-to-glass transition, can be attributed to the competition of these two hydrogen bonds. Moreover, it is well known that temperature and pressure are two important thermodynamic variables. On changing temperature, the interplay between these two distinct glass-forming mechanisms gives rise to the possibility of the system undergoing re-entrant and glass-to-glass transitions. However, although many valuable insights into these fascinating phase behaviours due to the variation of temperature have resulted from our previous experiments, to the best of our knowledge the effect of applied pressure on the KGT in a colloidal system still remains unexplored. Aiming at solving this puzzle, a series of SANS investigations have been launched recently. The preliminary experimental results suggest that, for the KGT in our micellar system, the effect of applying pressure is similar to that of reducing temperature.

It is well acknowledged that the KGT can be viewed as a mathematical singularity in the MCT equation [3]. A major prediction of MCT concerning the dynamics is, for a system with a given interaction potential, that on varying an external control parameter, such as the volume fraction or temperature, up to a certain value, the dynamics of the system will freeze and its associated relaxation time will diverge. A prerequisite in this argument is that the structure factor $S(k)$ derived from the given potential varies smoothly when the system transits from a liquid state to a nonergodic state. However, our SANS experimental results indicate that, instead of a smooth variation, a significant difference between $S(k)$ before the KGT (liquid) and after it (glass) is observed. From the evolution of $S(k)$ as a function of time, SANS results suggest that this discrepancy is due to the ageing effect introduced into the system during the measurement.

The paper is organized as follows: after giving the details of the micellar system that we study, we first present the experimental methodology of PCS measurement, the SANS intensity distribution analysis and the SANS scaling plots, then discuss the KGT of the micellar system, as a function of temperature and pressure, at different volume fractions, and report the first observation of the glass–glass transition and its end point in a colloidal system, and finally describe and discuss the pressure and ageing effects on these complex phase behaviours; we end with conclusions.

2. The L64/D_2O micellar system

The micellar system that we study is a triblock copolymer L64, a member of the Pluronic family, used extensively in industrial applications. After the necessary purification [18] to remove hydrophobic impurities, the polymer is dissolved in deuterated water (D_2O). Pluronic is made of polyethylene oxide (PEO) and polypropylene oxide (PPO). The chemical formula of

L64 is $(PEO)_{13}(PPO)_{30}(PEO)_{13}$; it has a molecular weight of 2990 Da. At low temperatures, both PEO and PPO are hydrophilic, so L64 chains readily dissolve in water, and the polymers exist as unimers. However, as the temperature increases there is a decrease in the probability of formation of hydrogen bonds between water and polymer molecules; PPO tends to become less hydrophilic faster than PEO. This creates an imbalance of hydrophilicity between the end block and the middle block of the polymer molecule and consequently the copolymer molecules acquire surfactant properties in the aqueous environment and self-assemble to form micelles. Thus the micellar formation is initiated at a well-defined critical micellar temperature–concentration (CMT–CMC) line. As the temperature increases further, water becomes progressively a poorer solvent for both PPO and PEO chains, and the effective micelle–micelle interaction becomes attractive. Evidence for the increased short range micellar attraction as a function of temperature comes from the existence of a lower consolute critical point at $C = 5.0$ wt% and $T = 330.9$ K [20] and a percolation line detected via a jump of the zero-shear viscosity of more than two orders of magnitude [22]. We have explored the dynamically arrested states and their structure in this micellar system, as a function of temperature at high volume fractions.

3. Experimental section

SANS measurements were performed at the NG7, 40 m SANS spectrometer in the NIST Center for Neutron Research, and at SAND station at the Intense Pulsed Neutron Source (IPNS) in Argonne National Laboratory. At NG7, incident monochromatic neutrons of wavelength $\lambda = 5$ Å with $\Delta\lambda/\lambda = 10\%$ were used. The magnitude of the wavevector transfer k ranges from 0.008 to 0.3 Å^{-1}. At IPNS, a pulse of white neutrons was selected with an effective wavelength range from 1.5 to 14 Å. At SAND all these neutrons are utilized by encoding their individual times of flight and their scattering angles determined from their detected positions on a 2D area detector. This configuration gives a reliable k-range covering from 0.004 to 0.6 Å^{-1}. The k-resolution functions of both of these SANS spectrometers are Gaussian and well characterized. The sample liquid was contained in a flat quartz cell with 1 mm path length.

A SANS hydraulic pressure cell is used to pressurize the L64/D_2O micellar solution. The pressure cell can reach pressures of 50 kpsi and temperatures from 260 to 360 K. Both pressure and temperature are computer controlled. Pressure scans at (constant) temperature can be performed to investigate the effect of applied pressure on the KGT.

The photon correlation spectroscopy (PCS) measurements were made at a scattering angle $\theta = 90°$, using a continuous wave solid state laser (Verdi-Coherent) operating at 50 mW ($\lambda = 5120$ Å) and an optical scattering cell of a diameter 1 cm in a refractive index matching bath. The intensity data were also corrected for turbidity and multiple-scattering effects. PCS data have been taken using a digital correlator with a logarithmic sampling timescale which allows an accurate description of the intermediate scattering function (ISF), from 1 μs up to 100 s. Following the method used for colloidal hard spheres [8] we measure the correlation function

$$g^{(2)}(k,\tau) = \langle\langle I(k,0)I(k,\tau)\rangle\rangle / \langle\langle I(k,0)\rangle\rangle^2 \tag{1}$$

where $I(k,\tau)$ is the intensity of light scattered at wavevector k and at a delay time τ. The first bracket denotes the time average, and the second bracket denotes the positional average over different parts of the sample. Since the system shows a structural arrest transition, and therefore a nonergodic behaviour, particular care has been taken in averaging over many different positions in the sample for the measurement of the long time part of the time correlation function. For each sample and each temperature we have performed more than

200 positional average measurements, observing a large scattering area corresponding to three or more independent Fourier components and changing the position of the sample in order to observe different scattering volumes. The ISF $g^{(1)}(k, \tau)$ can be obtained from equation (1) in a straightforward way using the Siegert relation.

3.1. SANS data analysis

The absolute intensity (in units of cm^{-1}) of the small angle neutron scattering from a system of mono-dispersed micelles can be expressed by the following equation:

$$I(k) = cN\left[\sum_i b_i - \rho_w v_p\right]^2 \overline{P}(k)S(k) \tag{2}$$

where c is the concentration of polymer (number of polymers cm^{-3}), N the aggregation number of polymers in a micelle, $\sum_i b_i$ the sum of coherent scattering lengths of atoms comprising a polymer molecule, ρ_w the scattering length density of D_2O, v_p the molecular volume of the polymer. $\overline{P}(k)$ is the normalized intraparticle structure factor calculated by the modified cap-and-gown model [16] and $S(k)$ the intermicellar structure factor of a spherical particle system interacting via an attractive square well potential with a repulsive hard core defined as

$$V(r) = \begin{cases} +\infty & \text{for } 0 < r < R' \\ -u & \text{for } R' < r < R \\ 0 & \text{for } r > R. \end{cases} \tag{3}$$

$S(k)$ is calculated analytically by solving the Ornstein–Zernike (OZ) equation in the Percus–Yevick (PY) approximation, for this square well potential, to first order in a series expansion in small ε [24] and the result for the structure factor is given as follows:

$$\begin{aligned}\frac{1}{S(Q)} = {} & 1 + 24\phi\left[\alpha f_2(Q) + \beta f_3(Q) + \frac{1}{2}\phi\alpha f_5(Q)\right] + 4\phi^2\lambda^2\varepsilon^2\left[f_2(\varepsilon Q) - \frac{1}{2}f_3(\varepsilon Q)\right] \\ & + 2\phi^2\lambda^2\left[f_1(Q) - \varepsilon^2 f_1(\varepsilon Q)\right] - \frac{2\phi\lambda}{\varepsilon}\left[f_1(Q) - (1-\varepsilon)^2 f_1((1-\varepsilon)Q)\right] \\ & - 24\phi\left[f_2(Q) - (1-\varepsilon)^3 f_2((1-\varepsilon)Q)\right]\end{aligned} \tag{4}$$

where $Q = kR$, $\phi = \frac{c\pi R^3}{6N}$,

$$\alpha = \frac{(1+2\phi-\mu)^2}{(1-\phi)^4}$$

$$\beta = -\frac{3\phi(2+\phi)^2 - 2\mu(1+7\phi+\phi^2) + \mu^2(2+\phi)}{2(1-\phi)^4}$$

$$\mu = \lambda\phi(1-\phi)$$

$$\lambda = \frac{6(\Delta - \sqrt{\Delta^2 - \Gamma})}{\phi}$$

$$\Delta = \tau + \frac{\phi}{(1-\phi)} = \frac{1}{12\varepsilon}\exp\left(-\frac{u}{k_B T}\right) + \frac{\phi}{(1-\phi)}$$

$$\Gamma = \frac{\phi(1+\phi/2)}{3(1-\phi)^2}$$

$$f_1(x) = \frac{1-\cos x}{x^2}$$

$$f_2(x) = \frac{\sin x - x\cos x}{x^3}$$
$$f_3(x) = \frac{2x\sin x - (x^2-2)\cos x - 2}{x^4}$$
$$f_5(x) = \frac{(4x^3-24x)\sin x - (x^4-12x^2+24)\cos x + 24}{x^6}.$$

This formula is accurate in the k region around the first diffraction peak for $\varepsilon < 0.05$ [23]. It is important to note that an absolute SANS intensity distribution in the liquid state can be calculated using equation (2) unambiguously with the four parameters N, ϕ, ε and T^*.

A SANS intensity distribution obtained from a 48.5 wt% micellar solution at 333 K is given in figure 3 to illustrate the model fitting. For sufficiently large k, the SANS absolute intensity decreases as k^{-4}, in agreement with Porod's law, as expected for a two-phase system with a sharp interface. The lower panel gives the normalized intraparticle structure factor $\overline{P}(k)$ (circles) and the interparticle structure factor $S(k)$ (squares) for this case. The observed SANS data are proportional to the product of these two functions. The fact that the first diffraction peak of $S(k)$ occurs in a relatively smooth tail part of $\overline{P}(k)$ implies that the interaction peak in the SANS intensity distribution is primarily reflecting the width of the first diffraction peak of $S(k)$.

3.2. The scaling plot of the SANS intensity distribution

The SANS intensity distribution from the L64/D_2O micellar system generally consists of a single, sharp interaction peak. We can assume that the system is characterized by a single length scale $\Lambda = \frac{1}{k_{\max}}$ where $k_{\max}$ is the peak position of the intensity distribution. It is well known that the absolute intensity in a two-phase system (the micelles and the solvent) is given by a 3D Fourier transform of the Debye correlation function $\Gamma(r)$. The Debye correlation function is a two-point correlation function of the local scattering length density in the system. In this case it must be of the form $\Gamma(\frac{r}{\Lambda})$ since Λ is the unique length scale in the system. Therefore

$$I(k) = \langle\eta^2\rangle \int_0^\infty \mathrm{d}r\, 4\pi r^2 j_0(kr)\Gamma\left(\frac{r}{\Lambda}\right) \tag{5}$$

where $\langle\eta^2\rangle$ is the so-called invariant of the intensity distribution.

We define $x \equiv \frac{r}{\Lambda} = k_{\max}r$ and $y \equiv \frac{k}{k_{\max}}$. It is straightforward to show that

$$\frac{k_{\max}^3 I(k)}{\langle\eta^2\rangle} = \int_0^\infty \mathrm{d}x\, 4\pi x^2 j_0(xy)\Gamma(x). \tag{6}$$

From the above equation, it can be seen that the scaled intensity $\frac{k_{\max}^3 I(k)}{\langle\eta^2\rangle}$ is a unique function of the scaled magnitude of the scattering vector, $y = \frac{k}{k_{\max}}$. Therefore, if we plot the scaled intensity distributions at different temperatures as a function of y, they should collapse onto one single master curve in a single-phase amorphous state.

It can be shown that [19]

$$\frac{k_{\max}^3 I(k)}{\langle\eta^2\rangle} \approx \frac{k_{\max}^3 S(k)}{\frac{1}{2\pi^2}\int_0^{k_1} k^2 S(k)\,\mathrm{d}k} \qquad \text{for } k \leqslant k_1. \tag{7}$$

That is, the scaled intensity is proportional to the interparticle structure factor $S(k)$ in the region of its first diffraction peak.

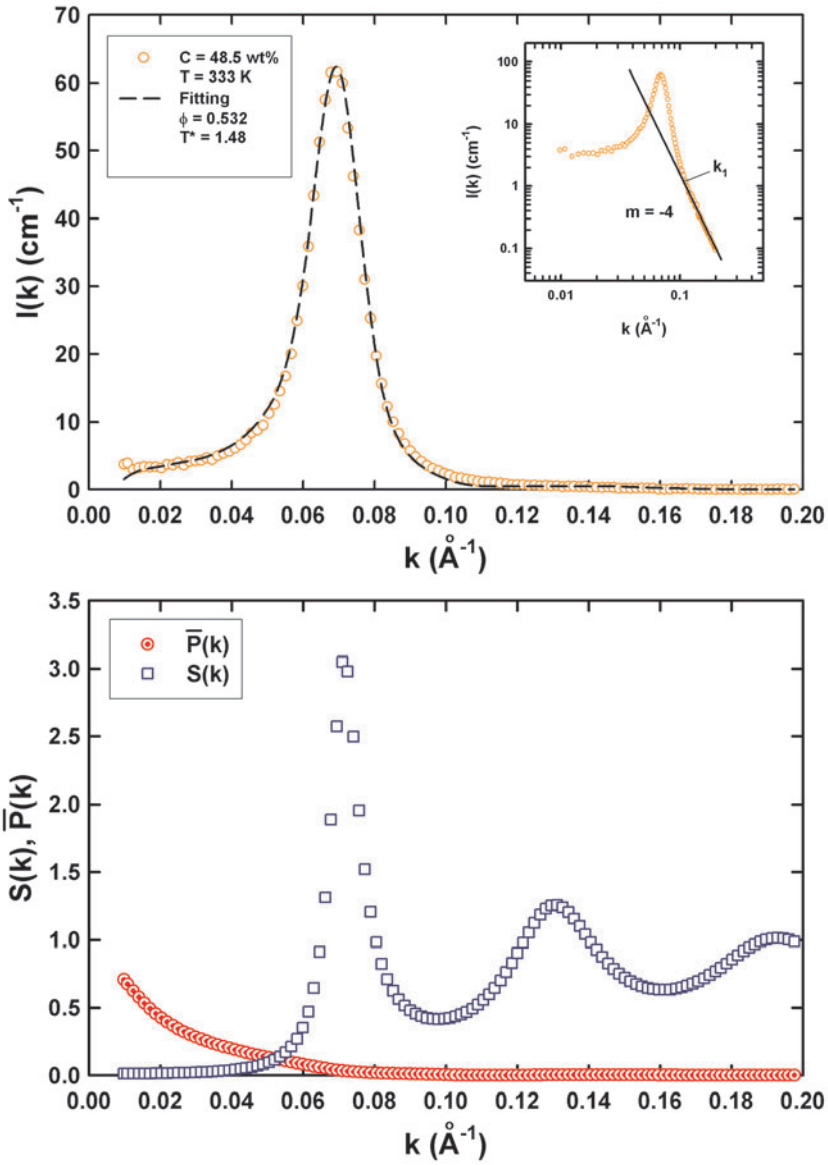

Figure 3. The upper panel shows the typical SANS intensity distribution on an absolute scale and its model fit taking into account the resolution correction. Symbols represent the experimental data and the dashed curve the theory convoluted with the resolution function. The inset gives the same data but plotted on a log–log scale. It can be seen that Porod's law is satisfied at large k, as is expected in a two-phase system with a sharp interface. The lower panel gives the normalized intraparticle structure factor $\overline{P}(k)$ (circles) and the interparticle structure factor $S(k)$ (squares) used to fit the data in the upper panel. $S(k)$ is calculated by solving the OZ equation with a square well intermicellar potential and $\overline{P}(k)$ is calculated using the modified cap-and-gown model [16] as the polymer segmental distribution function in a micelle. The observed SANS data are given by the product of these two functions and therefore it is clear that the interaction peak in the SANS data is primarily due to the first diffraction peak in the intermicellar structure factor.

4. Results and discussion

4.1. The intermediate scattering function (ISF) measured by photon correlation spectroscopy (PCS)

ISFs were measured for a set of volume fractions within the interval $0.525 < \phi < 0.546$, where the re-entrant phenomenon of the glass-to-liquid-to-glass transition, the glass-to-glass transition and the A_3 singular point were predicted for the case of $\varepsilon = 0.03$, as shown in figure 2. Figures 4(A) and (B) show ISFs obtained by PCS for two volume fractions, $\phi = 0.525$ and 0.535 respectively. On increasing temperature, the system, starting from a liquid state at a lower temperature, where the ISF decays to zero at long time, approaches a KGT, characterized by a diverging α relaxation time. At the KGT the ISF tends to a finite plateau at long time ($F(k, t \to \infty) = f_k > 0$). Just before this ergodic-to-nonergodic transition takes place, the ISF measured in an ergodic state exhibits a logarithmic relaxation (indicated by a straight line fit) at an intermediate time followed by a power-law decay before the final α relaxation sets in. This is in agreement with the MCT prediction. The nonergodic state ($T = 300$ K, for $\phi = 0.535$), as indicated by the ISF having a finite plateau at long time, represents the attractive glass for which the Debye–Waller factor (DWF; the height of the plateau) f_k is about 0.5. As discussed above, an important prediction of the MCT calculation for an AHS is the suggestion that there exists an attractive branch of the KGT line near the cusp singularity separating two different glass phases [25, 10]. Motivated by this prediction, we extended the study of the micellar system to higher temperatures. Starting from a glass state, upon increasing the temperature further, the measured ISF reveals a unexpected re-entry from the glass to the liquid state, as seen by the ISF again decaying to zero at higher temperatures.

The ISFs measured at $\phi = 0.538$ and 0.540 are given in figures 4(C) and (D). In addition to the volume fraction ϕ, the glass transition can be triggered by varying the effective temperature T^* as well. Due to the fact that the depth of the potential well $-u$ is temperature dependent and increases on heating to a certain extent, the effective temperature T^* actually decreases as temperature rises for a certain interval of temperatures. Variation of temperature thus makes the transition between two distinct types of glass possible. Because the long time limit of the ISF (DWF) reflects the degree of localization of the density fluctuation, these two different types of glass, if they have different degrees of local disorder, can be identified by their different values of the DWF. From figures 4(C) and (D) it is obvious that all the ISFs can be grouped into two distinct sets of curves having two different values of the DWF—one at $f_k = 0.5$ (attractive glass) and the other at $f_k = 0.4$ (repulsive glass). These two panels, 4(C) and (D), confirm the predicted glass-to-glass transition.

Figure 4(E) shows the ISFs measured at $\phi = 0.544$, which, according to MCT, is the end point of the predicted glass-to-glass transition line. Our measured ISFs verify this prediction, showing two nearly identical values of the DWF, for the two glassy states, with an average value of $f_k \sim 0.45$. Surprisingly, although the DWFs of these two types of glass are identical, there is a significant difference between the dynamics of their intermediate time relaxations (the β relaxation region).

The ISFs measured at $\phi = 0.546$, which is a volume fraction beyond the A_3 point, are shown in figure 4(F). This figure shows similar features to figure 4(E), with a merged DWF of $f_k \sim 0.4$. This indicates that beyond the volume fraction $\phi = 0.544$, the system exists in a repulsive glass state, suggesting critical point-like characteristics of the A_3 point.

4.2. Results of fitting SANS data

SANS experiments were performed on Pluronic L64/D_2O micellar solutions at different concentrations and temperatures. The experiments were carried out using the NG7 SANS

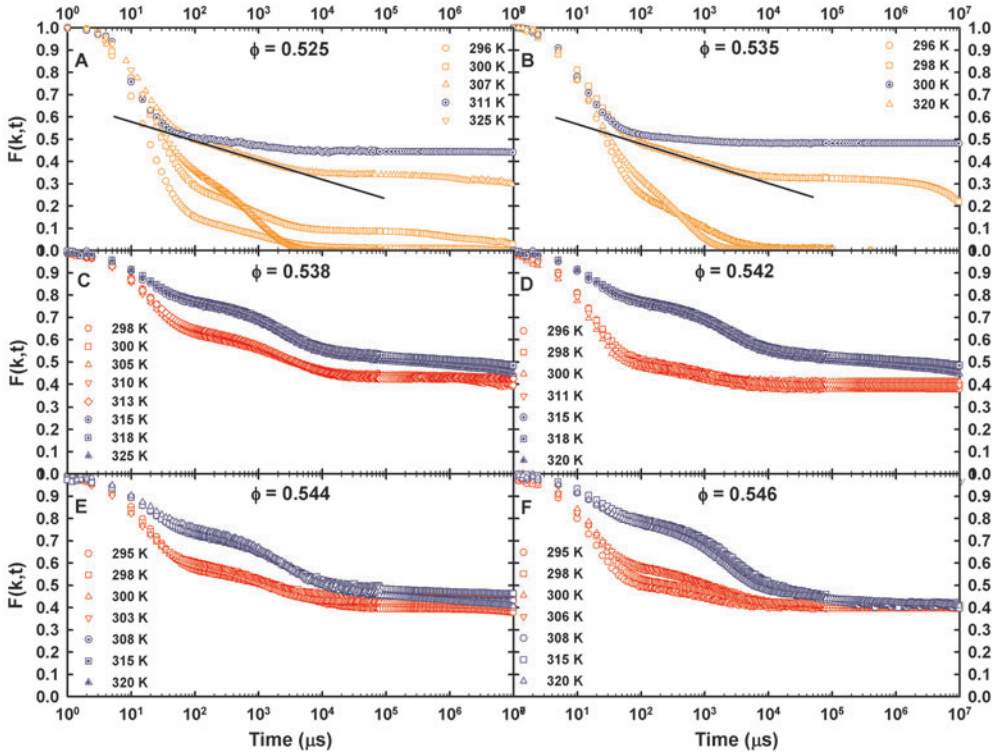

Figure 4. (A) and (B) represent ISFs measured at $\phi = 0.525$ and 0.535 respectively, where the liquid–attractive glass transition is found, as a function of temperature. In the liquid state, the long time limit of the ISF (DWF), f_k, is zero, while in the attractive glass state f_k is about 0.5. The structural arrest transition is thus characterized by a discontinuous change of f_k, called a bifurcation transition. The observed occurrence of a region of logarithmic time dependence, preceding the plateau region for the system in the ergodic state just before the transition, is highlighted by a straight line in the linear–log plots. (C) and (D) represent ISFs measured at $\phi = 0.538$ and 0.542. According to MCT, in this volume fraction range, there is a possibility of observing a glass-to-glass transition by varying the effective temperature T^*. Since the depth of the potential well $-u$ is temperature dependent and increases on heating, the effective temperature T^* actually decreases as temperature rises, making the transition from the repulsive glass to the attractive glass possible. By comparing the long time limits of the ISFs, the two different types of the glasses can be identified by their respective DWFs, $f_k^{\mathrm{A}} \sim 0.5$ and $f_k^{\mathrm{R}} \sim 0.4$. The reason for observing two different values of DWFs can be identified as the different degrees of localization of the density fluctuation having the wavenumber k for the two types of glasses. (E) gives ISFs measured at $\phi = 0.544$, where according to MCT, the long time limits of the ISFs of the two glasses become identical. In our measurements, the long time limit of the ISF of the attractive glass gradually decreases from 0.5 and gets closer to 0.4, the long time limit of the ISF of the repulsive glass. Although the DWFs of these two types of glass are almost identical, it is essential to recognize that there is a significant difference between the dynamics of their intermediate time relaxations. (F) gives ISFs measured at $\phi = 0.546$. At this volume fraction, the long time limit of the ISF of the attractive glass approaches close to 0.4, which is the long time limit of the ISF of the repulsive glass. This indicates that beyond the volume fraction 0.544, the two glasses merge into a single repulsive glass. Judging from (E) and (F), the experimentally determined volume fraction for the A_3 singularity lies somewhere between $\phi = 0.544$ and 0.546.

spectrometer at NIST Center for Neutron Research and the SAND station at IPNS, Argonne National Laboratory. Some of the experimental results as well as their theoretical fits are given in figure 5. Symbols are experimental data and the lines are the fits. The fits are on

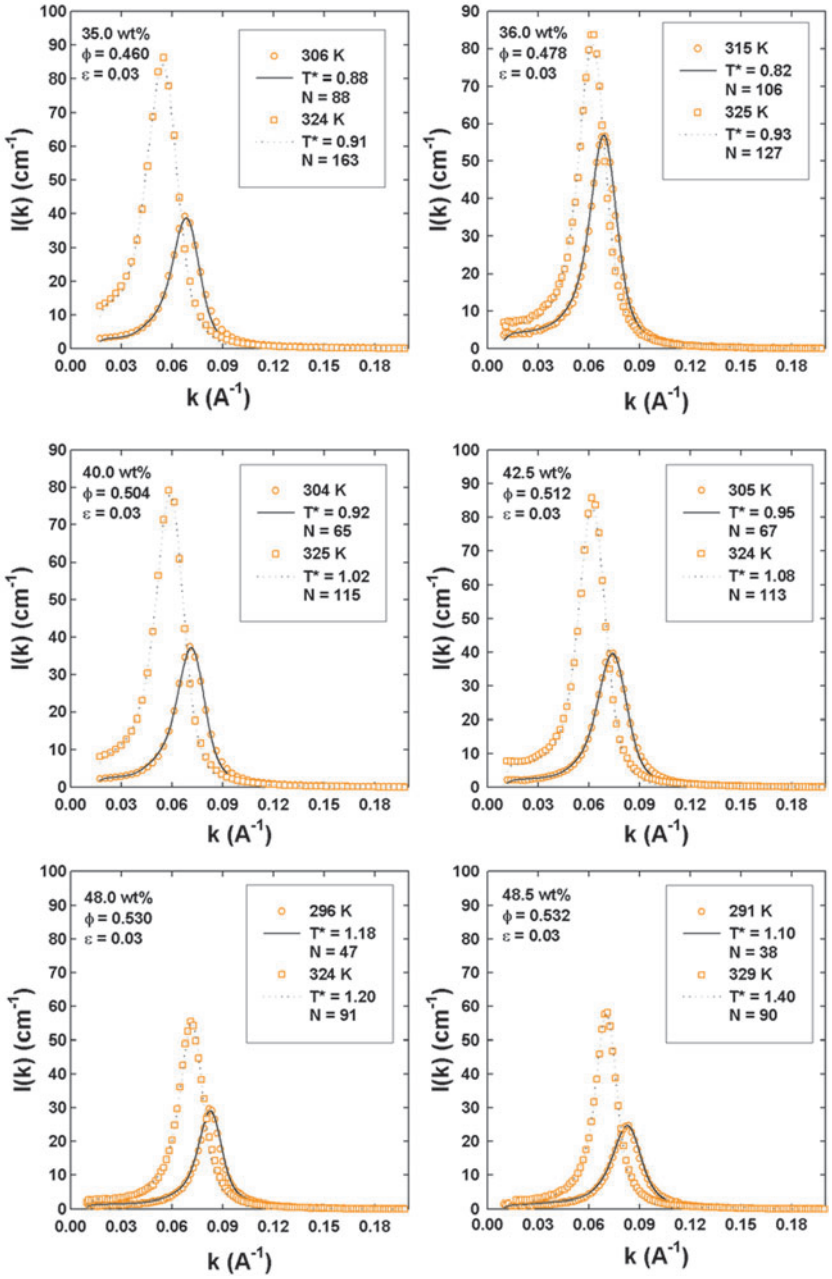

Figure 5. The theoretical fits to SANS data for Pluronic L64/D_2O micellar solutions at various concentrations and temperatures. Symbols are experimental data and the lines are the fits. The scattering intensities increase for the higher temperature liquid phase as compared to the lower temperature liquid phase and the position of the peak shifts toward smaller k due to the enhanced self-association as a consequence of increased hydrophobicity of the polymer segments at higher temperatures.

an absolute intensity scale taking into account the effects of the instrument resolution and the incoherent background. It can be seen that the peak intensity is generally higher for samples

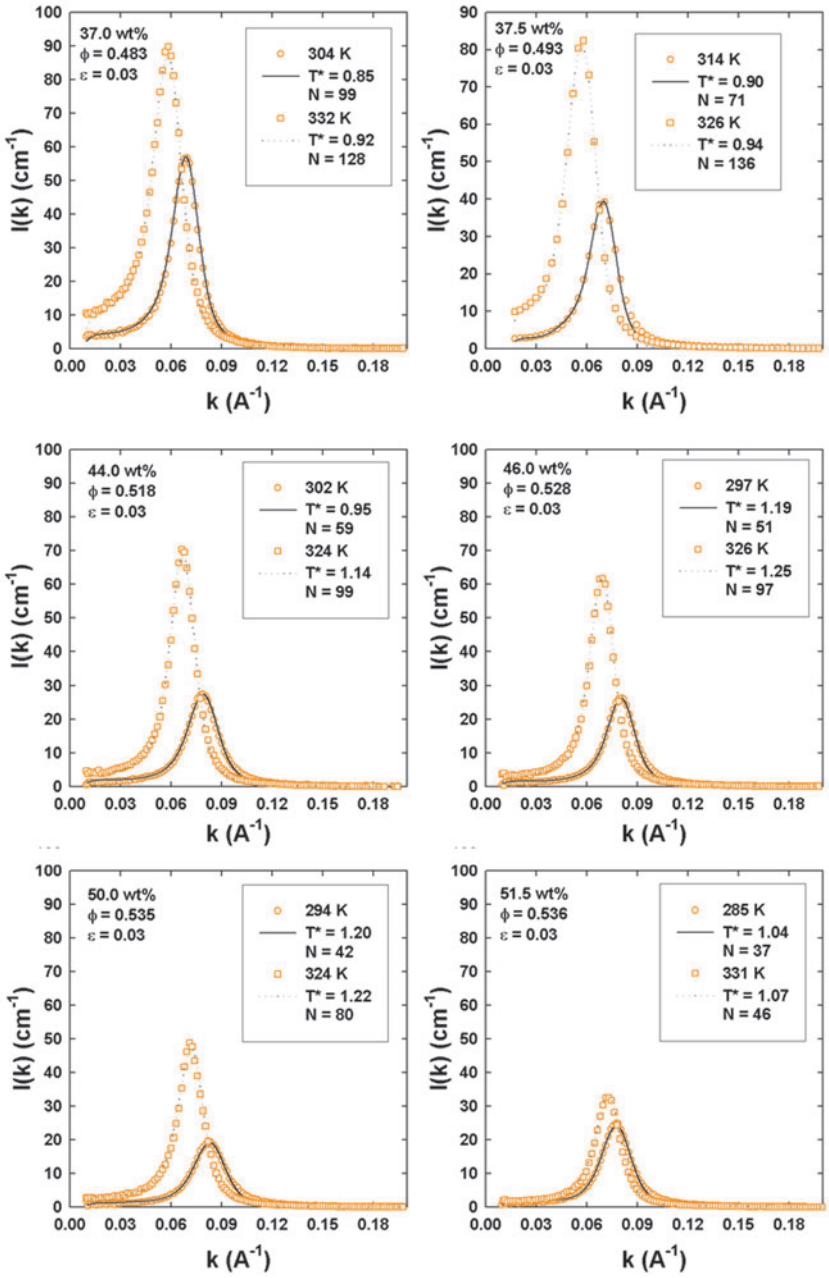

Figure 5. (Continued.)

in the higher temperature liquid phase. Furthermore, the position of the peak shifts toward smaller k as temperature increases. This is due to the enhanced self-association of the micelle (larger aggregation number) as a consequence of the increased hydrophobicity of the polymer segments at higher temperatures. It is important to note here that in spite of the micelle growth as temperature increases, SANS data analyses show that the volume fraction of the micelles remains constant, for a given weight fraction of L64, at all temperatures studied.

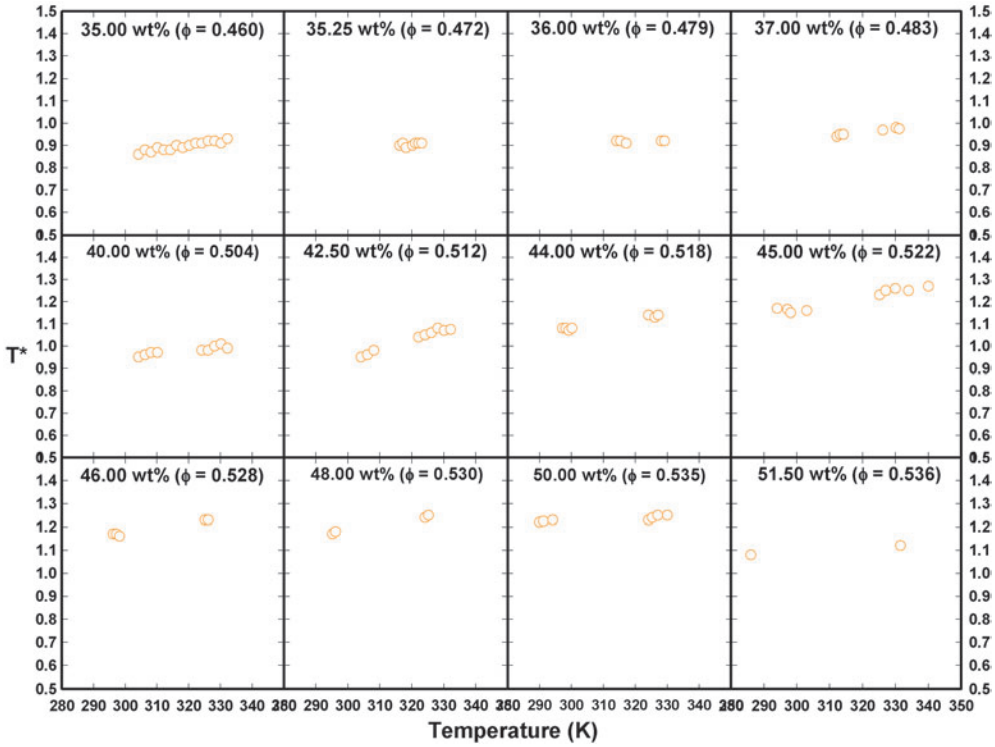

Figure 6. The effective temperature T^* of the liquid state as a function of temperature, obtain by fitting SANS intensity distributions for different concentrations. For the indicated concentrations, T^* generally increases as temperature increases, except in the glass region which appears as a gap in the figure.

Figure 6 summarizes the variation of the fitted effective temperature parameter T^*, as a function of temperature T, for several volume fractions studied. It can be seen clearly that as T increases, T^* increases also. There are no data shown in the glass regions, which appear as gaps in the plots, due to the lack of an appropriate theory for the structure factor of a system in a nonergodic state.

4.3. Scaling plots of SANS data

The mean particle separation distance which characterizes the unique length scale in the liquid state can best be visualized via a scaling plot. Figure 7 shows a scaling plot of a micellar solution at a polymer weight fraction of 35.0 wt% at a series of temperatures ranging from 304 to 322 K. All the scaled intensity distributions are temperature independent and indeed collapse into one single master curve. According to our measurement, this temperature independent scaled plot is observed for every polymer solution for which the polymer weight fraction is between 25.0 and 35.25 wt%. Figure 7 also indicates that the system is in the liquid state, because all the scaled peaks are considerably broader than the resolution function of the instrument. As we go above the concentration 35.25 wt%, the situation changes dramatically. As an example, figure 8 shows the scaling plots for the 45 wt% concentration sample at different temperatures. The volume fraction of micelles for this polymer concentration is determined by SANS data analysis to be at $\phi = 0.522$, independent of temperature. In view of the fact that the 2D

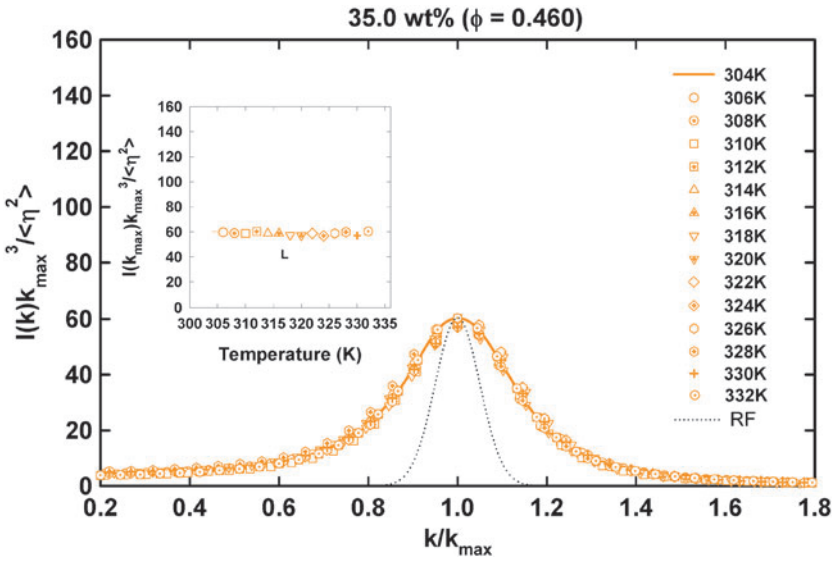

Figure 7. The scaling plot of the SANS intensity distributions of the micellar solution at $\phi = 0.460$ and at different temperatures. It is seen from the figure that the system is indeed characterized by a unique temperature dependent length scale. The fact that the scaling peak is considerably broader than the resolution function indicates that the system is in the liquid state. The inset shows the plot of the scaling height of all the scaled SANS intensity distributions as a function of temperature; it gives no sign of a phase transition.

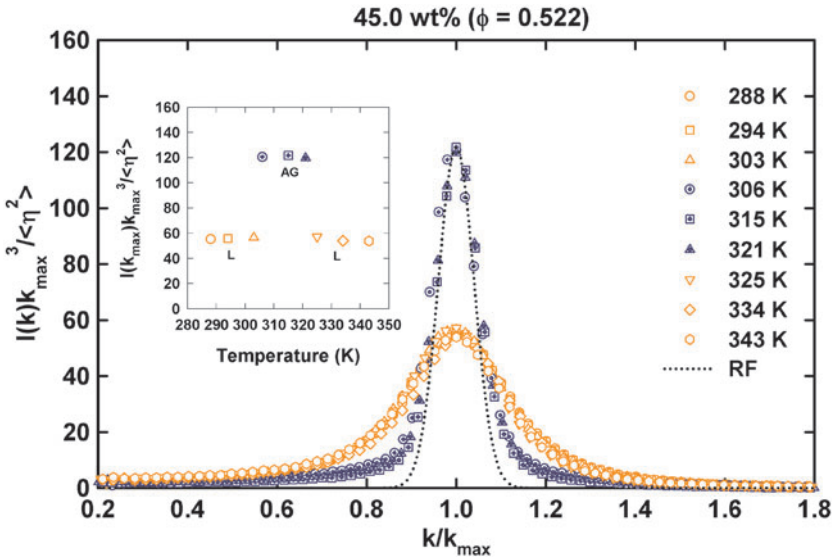

Figure 8. The scaling plots of SANS intensity distributions at $\phi = 0.522$, where the liquid-to-glass-to-liquid transition is observed, over a temperatures range spanning from 288 to 343 K. It is seen clearly that there are two distinct degrees of disorder (judging from the height and width of the peak), which depend on temperature. The inset gives the scaling height as a function of temperature. The variation of the peak heights indicates the re-entrant liquid-to-attractive glass-to-liquid transition.

SANS patterns show an isotropic ring, we conclude that the sample stays amorphous over the entire temperature range studied at this concentration. As mentioned before, the scaling peak

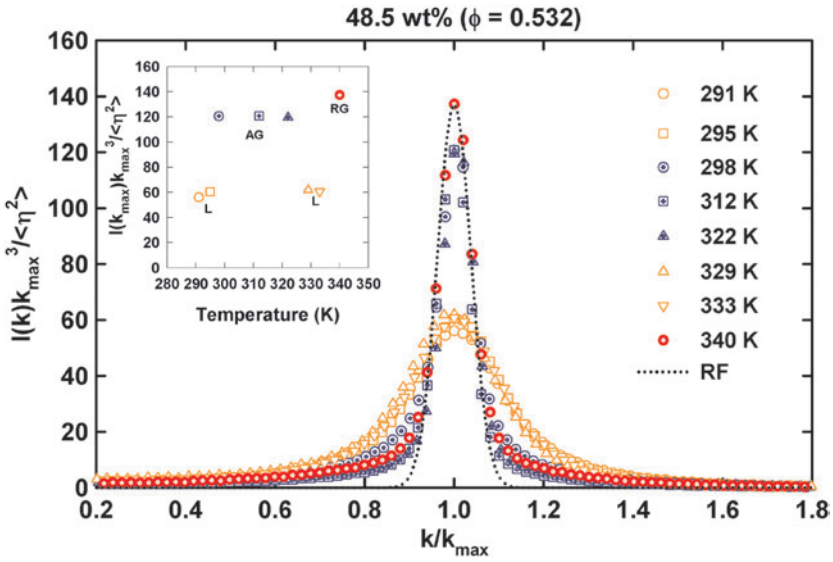

Figure 9. The scaling plots at $\phi = 0.532$, over a temperature range spanning from 290 to 340 K. This figure shows similar features to figure 8. However, as the temperature is increased to 340 K, another disordered state is observed. While the narrowest peak (340 K) is resolution limited, the slightly broader peak (298–322 K) is also nearly resolution limited but lower in intensity. From the inset given in the bottom panel, the liquid-to-glass-to-liquid-to-glass re-entrant transition can be seen clearly.

characterizes the position and the height of the first diffraction peak of $S(k)$. It is well known that the position of the first diffraction peak of $S(k)$ reflects the mean interparticle separation of the system and the height of the peak reflects the degree of local order surrounding a typical particle. Thus the height and the width of the scaling peak can be used to visualize the degree of local order surrounding a given particle in an amorphous state. Therefore, a sudden sharpening at a given temperature signals the onset of the liquid-to-amorphous solid transition. As one can see, there are two distinct degrees of disorder, that depend on temperature. While the narrower peak, which is resolution limited, represents the glassy state, the broader peak, which is much broader than the resolution, represents the liquid state with a broader distribution of the interparticle distances. This figure indicates that the system shows a re-entrant liquid-to-attractive glass-to-liquid transition as temperature increases. The sharpness of the scaling peaks which are resolution limited indicates that the nearest neighbour distance in the glassy state (ranging from 306 to 321 K) is more uniform than that in the liquid state (288–303 K, 325–343 K). The inset gives the peak height of the scaling plots as a function of temperature. The variation of the peak heights indicates the re-entrant liquid-to-attractive glass-to-liquid transition.

SANS intensity distributions and their scaling plots for a sample at 48.5 wt%, or $\phi = 0.532$, at a series of temperatures ranging from 291 to 340 K are given in figure 9. The scenario is similar to the previous example: a temperature dependent degree of disorder again characterizes the system. As the temperature rises, the system experiences a liquid-to-glass-to-liquid transition. However, in addition to all the similarities, when the temperature increases to 340 K the system is driven into another glassy state. The difference between these two disordered glassy states can be seen from their respective scaling peak heights: while the narrowest peak (340 K) is resolution limited, the slightly broader peak (298–322 K) is also nearly resolution

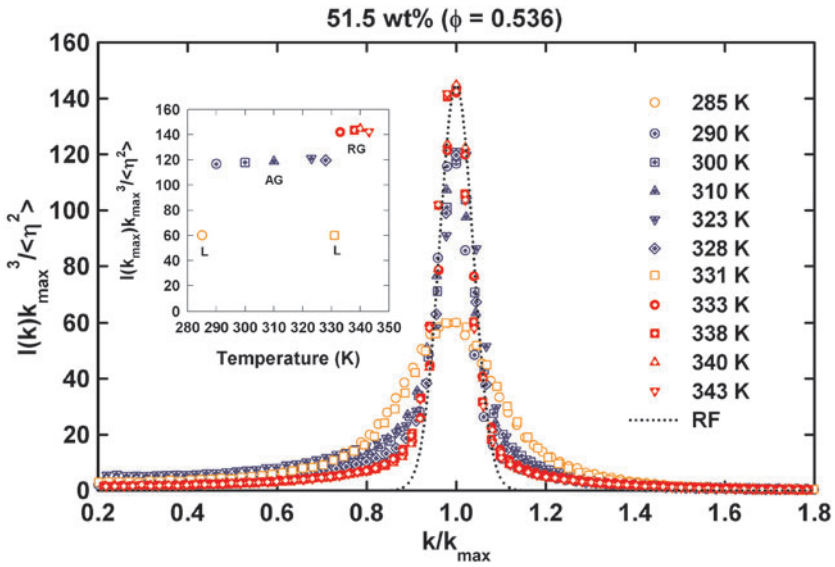

Figure 10. The scaling plots at $\phi = 0.536$, over a temperature range spanning from 285 to 343 K. This figure exhibits all the features found in figure 9. However, the high temperature liquid state is only observed at 331 K; when the temperature increases to 333 K, the system transits to the repulsive glass state. Figures 9 and 10 together give convincing evidence of the predicted re-entrant glass-to-liquid-to-glass transition. The only difference between them is that the temperatures of transition between different amorphous states are different. The inset shows the re-entrant transition more clearly.

limited but lower in scaled intensity. Since the difference in local structure of different states is reflected in their scaling plots, we conclude that the degrees of disorder are different for these two amorphous states. We can interpret this as showing that, on varying the temperature, the system shows a liquid-to-glass-to-liquid-to-glass transition.

Figure 10 gives the same plots, taken at a concentration of 51.5 wt%, or $\phi = 0.536$, for different temperatures. Generally it delivers the same message as figure 9: it shows the re-entrant transition. However, it can be seen that the temperatures of transition between different states for these two different volume fractions are different, especially in the high temperature region. For example, for the case of $\phi = 0.536$, the high temperature liquid state is only observed at 331 K. When the temperature increases to 333 K, the system transits to the repulsive glass state. The peak heights of the scaling plots as a function of temperature are given in the insets of figures 9 and 10. The temperatures of transition between different amorphous states can be visualized clearly from them. These two figures give firm evidence of the re-entrant glass-to-liquid-to-glass transition, which is in good agreement with the prediction of MCT for an AHS system. Furthermore, the KGT boundaries determined from SANS agree with the results obtained from the latest specific heat measurements [28].

According to the MCT calculations for an AHS with sufficiently short range attraction, a glass-to-glass transition is predicted [10]. Although transitions between different amorphous glassy states are not uncommon in pure substances [26], there has been no detailed investigation of the glass-to-glass transition in a micellar system so far except for some recent reports [16, 17, 19]. In combination with the PCS (see figures 4(C) and (D)), SANS provided concrete evidence of such a transition in a micellar system. In the SANS intensity distributions, taken at $\phi = 0.538$, given in figure 11, the much broader peaks (liquid state) disappear and

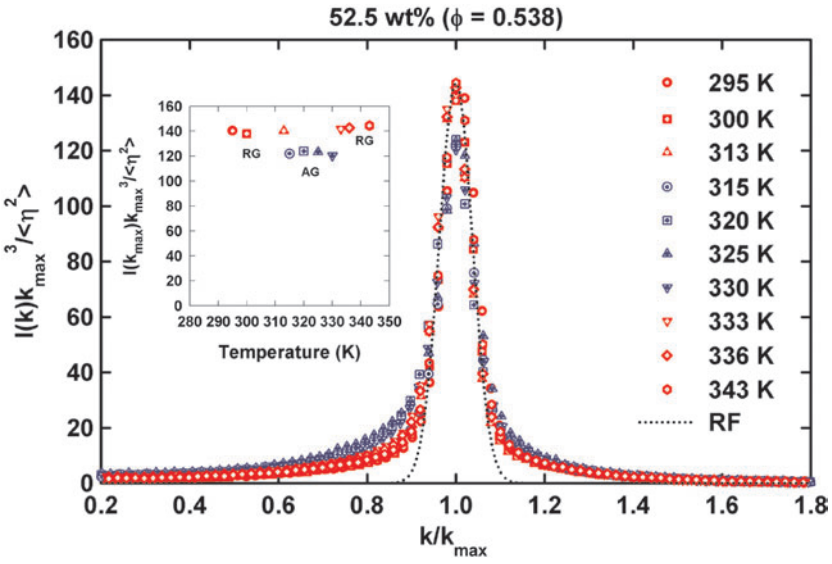

Figure 11. The scaling plots at $\phi = 0.538$, over a temperature range spanning from 295 to 343 K. It is observed that the much broader peaks (liquid state) disappear. Variation of temperature triggers the transition between the two amorphous solid states with different degrees of disorder. The variation of the peak heights of the scaling plots as a function of temperature given in the inset shows a re-entrant repulsive glass-to-attractive glass-to-repulsive glass transition for the first time.

variation of temperature triggers the transition between the two amorphous solid states with different degrees of disorder. With increasing temperature, the variation of the peak heights of the scaling plots given in the inset shows a re-entrant repulsive glass-to-attractive glass-to-repulsive glass transition.

Perhaps the most important prediction for the AHS system is the existence of the end point of the glass-to-glass transition line, the so-called A_3 singularity. Comparing with the critical point of the equilibrium states, a certain degree of similarity can be found. Therefore, it is intriguing to speculate on the extent to which one can draw an analogy between the A_3 singularity and the ordinary equilibrium critical point. In the case of $\varepsilon = 0.03$, the volume fraction of the A_3 point is predicted to be $\phi(A_3) = 0.544$. The SANS intensity distribution and its associated scaling plot are shown in figure 12. As one can see, all the scaling intensity curves collapse onto one single master curve, indicating that the first diffraction peaks of the structure factor for all states are identical. This suggests that the local structures of the two glasses are identical. The inset given in the bottom panel shows that all the scaling peaks have identical height (about 140), indicating that the two glasses do indeed have same degree of local order.

On increasing ϕ further to 0.546 (figure 13), all the scaled intensities are again characterized by a unique temperature independent length scale and collapse onto one single master curve, independent of temperature, showing identical local structures of the two glasses. This is proof that the MCT predictions are accurate.

Figure 14 summarizes the essential results of the extensive SANS and PCS data analysis. It contains the known equilibrium, liquid-to-hexagonal crystalline phase boundary (solid curve) [27], the experimentally determined KGT lines (dash curves) and the phase points where parts of the experimental data are taken (symbols). This figure gives several important pieces of information about this system: first, only the metastable attractive glass is observed

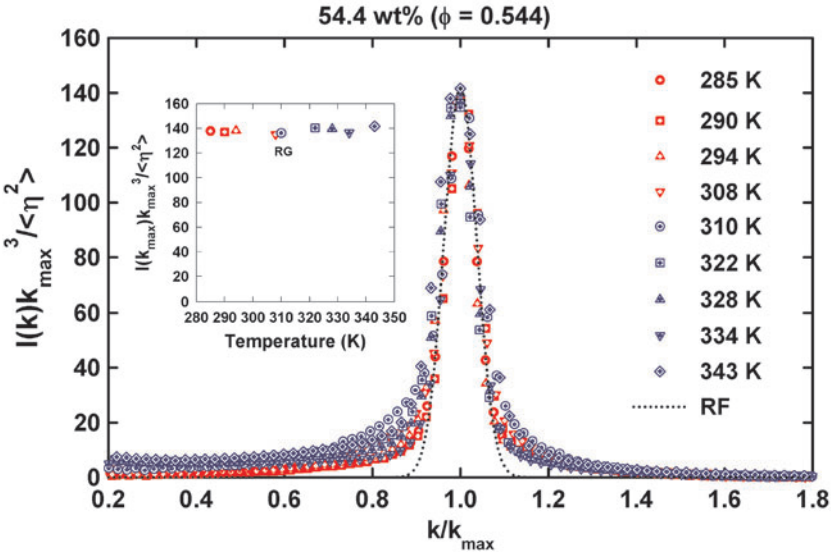

Figure 12. The scaling plots of SANS intensities at $\phi = 0.544$, which is predicted to be the volume fraction where the A_3 singularity point is located, over a temperature range spanning from 285 to 343 K. The inset given in the bottom panel shows that all the scaling peaks have identical height (about 140), indicating that the two glasses do indeed have the same degree of local order.

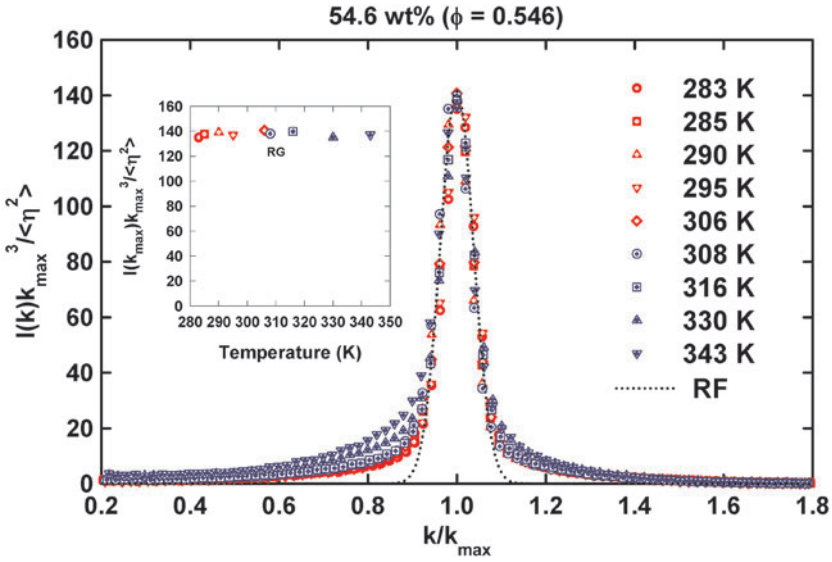

Figure 13. The scaling plots of SANS intensities at $\phi = 0.546$, a volume fraction beyond the A_3 point, over a temperature range spanning from 283 to 343 K. Like in figure 12, all the scaled intensities are again characterized by a unique length scale and collapse onto one single master curve which is independent of temperature, showing identical local structures of these two glasses.

within the region where the true lowest free energy state is the hexagonal liquid crystalline phase; next, the repulsive glass only exists in the region where the volume fraction is larger than 0.536. It is interesting to see that there is a pocket of the attractive glass embedded in between

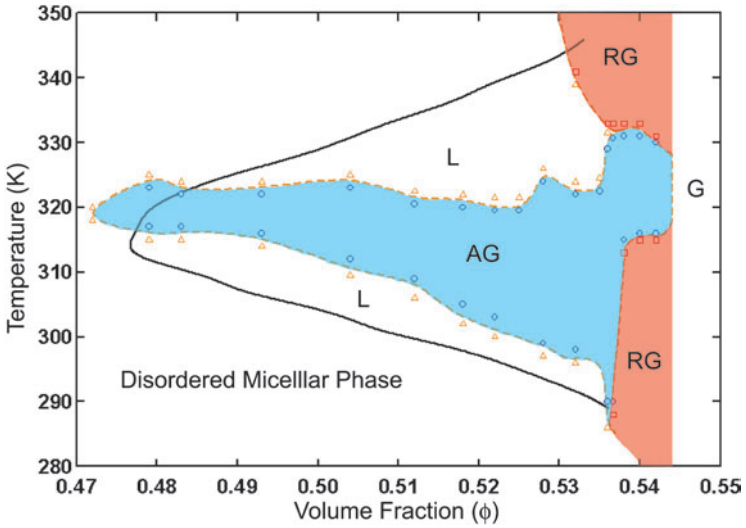

Figure 14. The experimental phase diagram of the L64/D_2O micellar system. The solid curve represents the equilibrium phase boundary of disordered micellar liquid states and the hexagonal liquid crystalline states [27]. The dashed curve gives the kinetic glass transition boundary which is determined by SANS and PCS. The symbols represent the phase points where parts of the experimental data were taken. The triangles represent the liquid state (L), the circles the attractive glass (AG), the squares the repulsive glass (RG). Within the region where the true ground state is the hexagonal liquid crystalline phase, only the metastable attractive glass is observed. The repulsive glass is found in the region where the volume fraction is larger than 0.536. Furthermore, the two different glasses become identical in local structure and the long time dynamics where the volume fraction exceeds ϕ (that is, A_3) is 0.544.

two separate repulsive glass regions spanning the volume fraction range between 0.536 and 0.544, where the re-entrant glass-to-glass transition is observed. From figures 4, 12 and 13, the two different glasses become identical in local structure and long time dynamics at a volume fraction $f(A_3) = 0.544$ or greater. Furthermore, judging from the DWF and the peak height of the scaled intensity, the merged identical glassy state is the repulsive glass.

It is well known that temperature and pressure are variables used to manipulate the phase behaviour in colloidal systems. For the L64/D_2O micellar system, our SANS and PCS experiments show that the KGT and several associated phase behaviours can be induced by varying the temperature. However, the response of the system to the applied pressure is still uncertain and interesting to pursue. Figure 15 gives SANS intensity distributions and their model fitting (upper panel) obtained at 44.0 wt% and 326 K and their associated scaling plots (lower panel), as a function of applied pressure. As the applied pressure increases, the SANS intensity keeps decreasing and the position of the peak shifts toward larger k. However, the scaling plots suggest that the system remains in the liquid phase over the whole pressure range. The extracted fitting results are given in figure 16: as pressure increases, the aggregation number N becomes smaller; that is, the size of the micelle reduces. The reducing micellar self-association can be explained as follows: in the presence of high applied pressure, the hydrogen bonding between D_2O molecules and micellar corona regions is partially destroyed. As a consequence, the decreased hydrophilicity in the corona region makes the contrast in hydrophobicity between the PPO core and the PEO corona less significant. Therefore it induces removal of D_2O molecules out of the corona region (H decreases) and hence makes the corona region less penetrable (ε decreases). The short range attraction between micellar

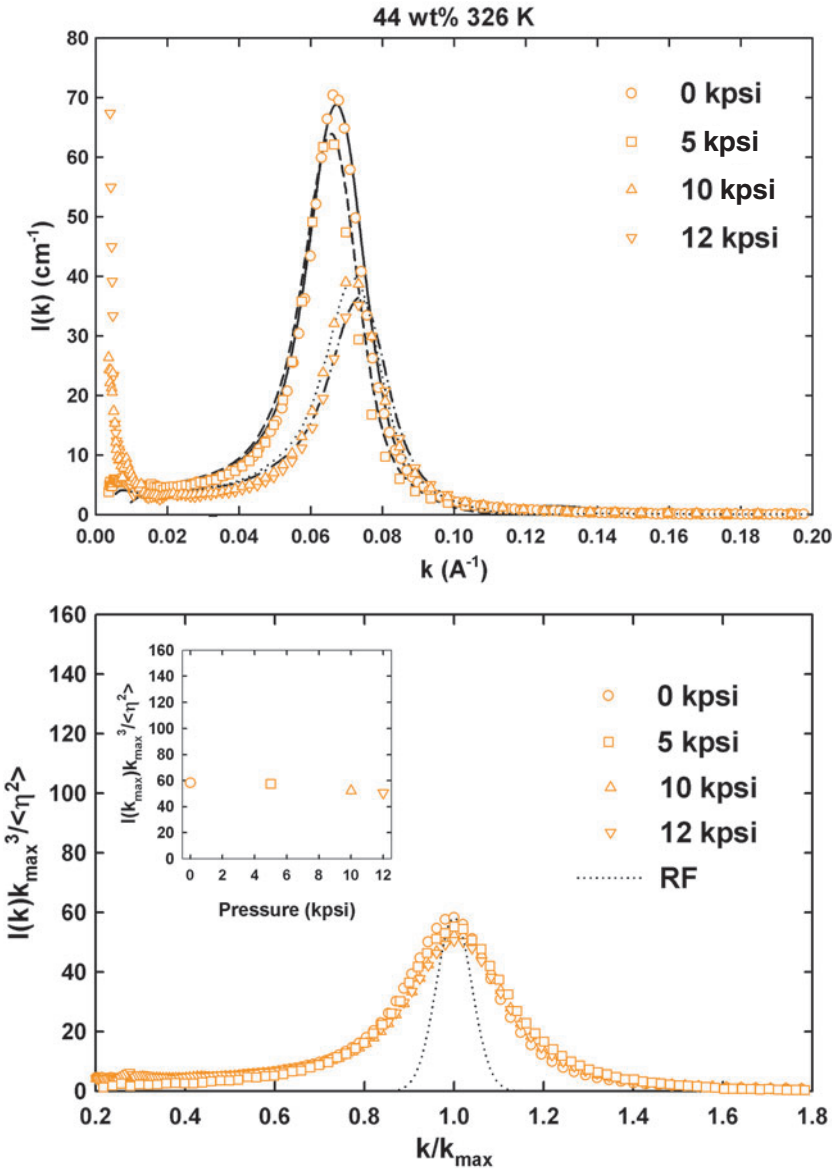

Figure 15. The SANS intensity distributions and their associated scaling plots at 44 wt%, 326 K, over a pressure range spanning from 0 to 12 kpsi. Symbols are the experimental data; the curves are the theory convoluted with the resolution function.

corona regions is thus enhanced accordingly (u increases). Compare with figure 5; it is clear that at constant temperature, increasing applied pressure has a similar effect to reducing temperature at constant pressure.

Provided with the structure factor derived from a given potential, MCT calculations have successfully predicted the discrete transition in the liquid state, namely the structural arrest transition. Due to the nonergodic nature of the glassy state, the analytical structure factor of the arrested state is unavailable. Therefore, a major assumption in MCT calculations is that,

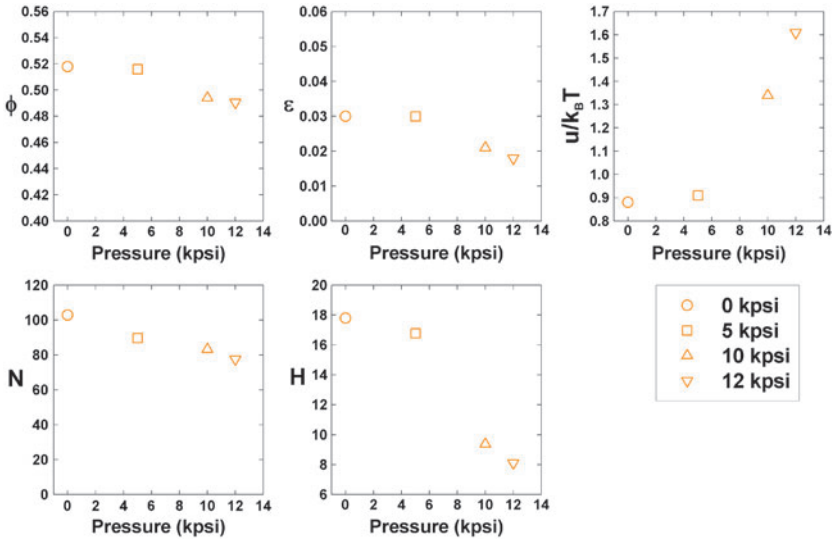

Figure 16. The volume fraction of micelles ϕ, fractional well width ε, depth of the short range attractive well u, aggregation number N and hydration number H for liquid states as a function of pressure, obtained by fitting the SANS intensity distributions for L64 at weight fraction 44 wt%, 326 K, at different pressures. For the concentrations indicated, ϕ, ε, N and H generally decrease as pressure increases. However, u increases as pressure increases.

when the KGT is triggered by varying the external control parameters, there is no significant difference in local structure. However, from our SANS experiments, on crossing the KGT boundaries at various temperatures for all the volume fractions studied, instead of smooth change in the structure factor, a significant difference is observed. As an example, an evolution of the structure factor as a function of time is given in figure 17. Initially, the sample is held in the liquid state (303 K, 1° away from the KGT line); then it is transferred to another thermal bath (306 K), which drives the sample from the liquid state to the attractive glass state. The top panel gives the associated scaling plots of the SANS intensity distributions and the height of the scaling peaks is given in the bottom panel. As predicted by the MCT, the structure factor in the glassy state is identical to that in the liquid state. However, as time evolves, the scaling height increases gradually from 60 to 120 (within 5 min), corresponding to a structure factor which cannot be derived from the equilibrium liquid theory. Therefore, the deviation between the MCT and our SANS experiments can be explained as follows: our SANS data are reflecting the effect of ageing of the sample on the timescale of our measurements.

5. Conclusion

We use PCS to show that the L64/D_2O micellar system follows the overall structural arrest transition behaviour predicted by MCT, calculated using a square well potential with a short range attraction relative to the micellar size. In particular, we show experimentally the existence of a glass-to-glass transition line which starts at point C^* (see figure 2), where the two glass phases and the liquid phase coexist, and ends at point A_3, where the two glass phases merge [16, 17, 19]. With this model potential, we are able to extract the corresponding volume fraction for a certain polymer weight fraction by SANS model fitting and therefore pinpoint the exact volume fractions where the C^* point and the A_3 singularity are located, and

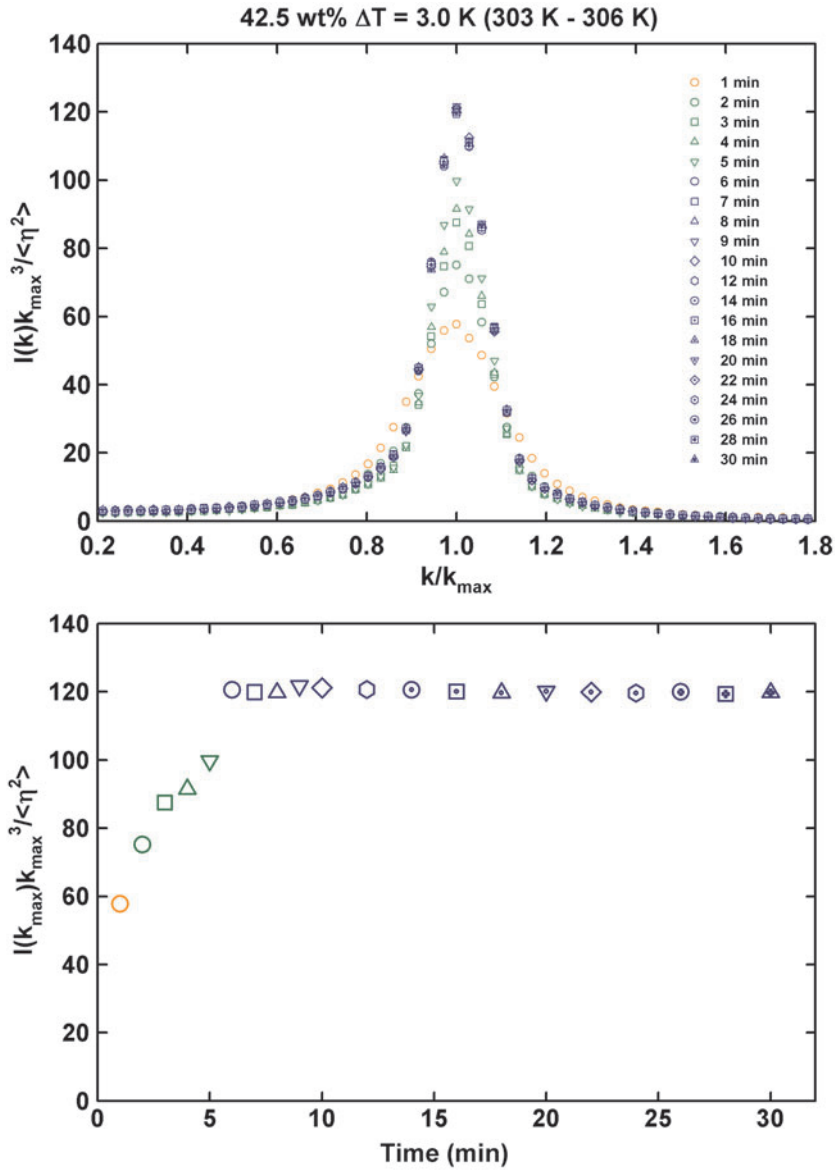

Figure 17. The upper panel gives the scaling plots of SANS intensities at $c = 42.5$ wt% for the ageing experiment (see the text for the details); the height of the scaling peak as a function of ageing time is given in the bottom panel.

map out the whole KGT boundaries in the L64/D_2O micellar system. The SANS experiment further shows that while the local structures of the attractive and the repulsive glasses are in general different, they become identical at the predicted volume fraction of the A_3 singularity, independent of temperature. However, our PCS results indicate that the relaxations of the two glasses are different in the intermediate time region even at the A_3 point.

Furthermore, analysis of the SANS experimental results obtained from a pressure range at constant temperature suggests that, at a certain temperature, the response of the KGT to the

increasing applied pressure is qualitatively similar to that of the decreasing temperature when the pressure is constant. Most importantly, due to the applied pressure, the depth of the short range attraction increases and the extent of the short range attraction decreases.

Finally, SANS reveals that when the system transits from a liquid state into a glassy state, initially the structure factor in the glassy state is similar to that of the liquid state, which is consistent with the assumption of MCT. Therefore, we conclude that the distinct differences in local structure observed in an extensive set of SANS intensity distributions are due to the ageing effect occurring during the measurement time.

Acknowledgment

The research at MIT is supported by a grant from the Materials Science Division of the US DOE, DE-FG02-90ER45429. The research in Messina is supported by INFM-PRA98 and MURST-PRIN2000. This work benefited from the use of IPNS funded by the US DOE, BES under contract W-31-109-ENG-38 from the University of Chicago and the support of CNR, NIST, US DOC, in providing the NG7 40 m SANS spectrometer used in this work. We are grateful to Dr Charles J Glinka and Mr Deny Wozniak for technical assistance. SHC would like to acknowledge fruitful exchange of ideas through the EU supported Marie Curie Network on Arrested Matters.

References

[1] Everett D H 1988 *Basic Principles of Colloid Science* (Letchworth: Royal Society of Chemistry)
[2] Dawson K 2002 *Curr. Opin. Colloid Interface Sci.* **7** 218
[3] Götze W 1991 *Liquids, Freezing and the Glass Transition* ed J P Hansen, D Levesque and J Zinn-Justin (Amsterdam: North-Holland)
[4] Götze W and Sjögren L 1992 *Rep. Prog. Phys.* **55** 241
[5] Götze W 1999 *J. Phys.: Condens. Matter* **11** A1
[6] Pusey P N and van Megen W 1987 *Phys. Rev. Lett.* **59** 2083
[7] Fuchs F 1995 *Transp. Theory Stat. Phys.* **24** 855
[8] van Megen W and Underwood S M 1994 *Phys. Rev.* E **49** 4206
[9] Bartsch E, Antonietti M, Schupp W and Sillescu H 1992 *J. Chem. Phys.* **97** 3950
[10] Dawson K, Foffi G, Fuchs M, Götze W, Sciortino F, Sperl M, Tartaglia P, Voigtmann Th and Zaccarelli E 2001 *Phys. Rev.* E **63** 01140
[11] Bergenholtz J and Fuchs M 1999 *Phys. Rev.* E **59** 5706
[12] Bergenholtz J and Fuchs M 1999 *J. Phys.: Condens. Matter* **11** 10171
[13] Eckert T and Bartsch E 2002 *Phys. Rev. Lett.* **89** 125701
[14] Pham K N, Puertas A M, Bergenholtz J, Egelhaaf S U, Moussaid A, Pusey P N, Schofield A B, Cates M E, Fuchs M and Poon W C K 2002 *Science* **296** 104
[15] Mallamace F, Gambadauro P, Micali N, Tartaglia P, Liao C and Chen S H 2000 *Phys. Rev. Lett.* **84** 5431
[16] Chen W R, Chen S H and Mallamace F 2002 *Phys. Rev.* E **66** 021403
[17] Chen S H, Chen W R and Mallamace F 2003 *Science* **300** 619
[18] Chen S H, Liao C, Fratini E, Baglioni P and Mallamace F 2001 *Colloids Surf.* A **183–185** 95
[19] Chen W R, Mallamace F, Glinka C J, Fratini E and Chen S H 2003 *Phys. Rev.* E **68** 041402
[20] Liao C, Choi S M, Mallamace F and Chen S H 2000 *J. Appl. Crystallogr.* **33** 677
[21] Lemaire B, Bothorel P and Roux D 1983 *J. Phys. Chem.* **87** 1023
[22] Lobry L, Micali N, Mallamace F, Liao C and Chen S H 1999 *Phys. Rev.* E **60** 7076
[23] Foffi G, Zaccarelli E, Sciortino F, Tartaglia P and Dawson K A 2000 *J. Stat. Phys.* **100** 363
[24] Liu Y C, Chen S H and Huang J S 1996 *Phys. Rev.* E **54** 1698
[25] Fabbian L, Götze W, Sciortino F, Tartaglia P and Thiery F 1999 *Phys. Rev.* E **59** R1347
[26] Ponyatovsky E G and Barkalov O I 1992 *Mater. Sci. Rep.* **8** 147
[27] Zhang K Z, Lindman B and Coppola L 1995 *Langmuir* **11** 538
[28] Mallamace F, Ferrari C, Mazzaglia A, Salvetti P, Tombari E and Chen S H 2004 at press